Article

Synthesis, Characterization, and Physicochemical Properties of New [Emim][BF₃X] Complex Anion Ionic Liquids

Ji-Jun Zeng, Bo Zhao, Yu An, Xiao-Bo Tang, Sheng Han, Zhi-Qiang Yang, Wei Zhang,* and Jian Lu*

Read Online

ACCESS | Metrics & More | Article Recommendations | SI Supporting Information

ABSTRACT: A new series of complex anion ionic liquids (ILs) [Emim][BF₃X] (X = CH₃SO₃, EtSO₄, HSO₄, Tosylate) were synthesized and characterized by nuclear magnetic resonance, elemental analysis, differential scanning calorimetry analysis, and thermogravimetry. The physicochemical properties of these ILs, such as density, viscosity, conductivity, and surface tension, were measured and correlated with thermodynamic and empirical equations in the temperature range of 293.15−358.15 K under ambient conditions, and the thermal expansion coefficient, standard molar entropy, lattice potential energy, viscosity activation energy, surface enthalpy, and surface entropy were further calculated from experimental values. According to the temperature-dependent viscosity and conductivity, [Emim][BF₃X] ILs follow the Walden rule, and they are classified as "good (or super) ionic liquids".
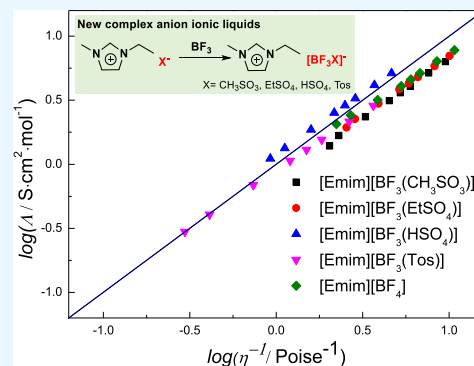
1. INTRODUCTION

Ionic liquids (ILs), a liquid composed of entire ions with low melting temperatures (below 100 °C), represent a special category of functional materials. The unique properties of ILs, including extremely low vapor pressure, tunable structure, excellent thermal and chemical stability, and high solvent power for organic and inorganic compounds, make them have potential applications in electrochemistry, organic synthesis and catalysis, separations, and biotechnology.[1,2]

The third-generation ILs, defined as "Task-specific" ILs, possess tunable physical and chemical properties according to a given task or the desired application.[3,4] In most instances, the fundamental chemical properties are defined by the choice of the anion (e.g., hydrophobic/hydrophilic nature, good/bad conductivity, low/high viscosity, glass forming, gas solubility, and many others),[5] while the choice of the cation allows these properties to be fine-tuned. Therefore, it is particularly important to discover new anions or modify existing anions to introduce new or improved properties or special combinations of properties.[6]

To search anions for "task-specific" ILs, the common strategy is to substitute existing anions, such as $[BF_4]^-$, $[PF_6]^-$, and $[NTf_2]^-$, by various functional groups including C_nF2_{n+1}, C_nH_{2n+1}, CN and Cl. Substituting one of four fluorine atoms in the $[BF_4]^-$ anion leads to nonsymmetric anions of the $[RBF_3]^-$ type. New ILs with alkyl(alkenyl)trifluoroborate ($[BF_3(C_nH_{2n+1})]^-$),[7] polyfluoroalkyltrifluoroborate ($[BF_3(C_nF_{2n+1})]^-$),[8] trifluorochloroborate ($[BF_3Cl]^-$),[9] or aryltrifluoroborate ($[ArBF_3]^-$)[10] anions and diverse cations have been synthesized. The replacement of fluorine atoms in the $[RBF_3]^-$ anion by cyano groups provides polyfluoroalkyl-cyanoborate ($[RBF_{3-x}(CN)_x]^-$ ($x = 1-3$)) anions.[11] Similarly, replacing three fluoride ions in the $[PF_6]^-$ anion by perfluoroethyl groups yields tris(pentafluoroethyl)-trifluorophosphate ($[FAP]^-$) anion.[12] Based on the $[NTf_2]^-$ anion, several analogous amide anions, such as bis-{(pentafluoroethyl)sulfonyl}amide ($[NDf_2]^-$),[13] bis{bis-(pentafluoroethyl)phosphinoyl}amide($[NPf_2]^-$),[14] and bis-(fluorosulfonyl)amide anions,[15] have been reported. The chemical structures of some selected modified anions are presented in Figure 1. Furthermore, the introduction of asymmetric structural fragments usually endows these modified anions with specific physicochemical properties, such as lower melting point, lower viscosity, and higher conductivity. However, the preparation of these modified anions involves highly hazardous processes (F₂ fluorination, electrochemical fluorination),[16,17] with expensive reagents (AlkLi, perfluori-nated hydrocarbons).[18,19] These factors make ILs based on these modified anions expensive and restrict the further development of these ILs. Until now, these ILs are still classified as "unusual anion-based ILs", although they were synthesized 20 years ago.[20]
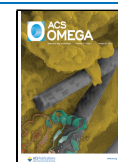
Herein, a new effective strategy by designing anions for "Task-specific" ILs was first proposed via hybrid complexing Lewis fluoroacids MFₙ with common ILs (Q⁺X⁻) to obtain
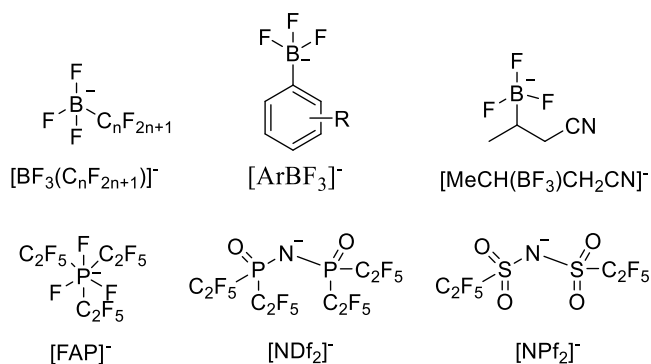
Figure 1. Chemical structures of some of the selected modified anions.

complex anion ILs ($Q^+[MF_nX]^-$).[21] This strategy significantly modifies the structural properties of the anion $[X]^-$, including symmetry, donor ability, and conformational degrees of freedom, and allows one to control the strength of the Coulomb interactions, hydrogen bonding, dispersion, and dipole–dipole interactions in the ILs,[22] thus obtaining ILs with specific physicochemical properties. In the present work, new $[Emim][BF_3X]$ complex anion ILs were obtained by complexing BF_3 with $[Emim][X]$. The synthesized ILs were then characterized by nuclear magnetic resonance (NMR), elemental analysis, differential scanning calorimetry (DSC) analysis, and thermogravimetry (TGA). Several important physical properties, such as density, viscosity, conductivity, and surface tension, were measured at the specified temperature under atmospheric conditions.

2. EXPERIMENTAL SECTION

2.1. General Information. All of the chemicals were purchased from Alfa Aesar, Macklin, Sigma-Aldrich, and TCI as listed in Table 1. Before the experiments, all ionic liquids were dried under vacuum at 60–90 °C for 24 h to reduce the impact of water impurity, while dichloromethane was dried over activated 3A molecular sieves for several days. The water content of every chemical was determined by Karl Fischer titration (Mettler Toledo DL31), and the mean of three replicate measurements was reported.

BF$_3$ was handled in a vacuum line constructed of SUS316 stainless steel. Nonvolatile materials were handled under the N$_2$ atmosphere in a glovebox. A poly(tetrafluoroethylene)

(PTFE)-lined stainless steel reactor combined with a stainless steel valve was used as a reaction vessel. All sample preparation was done with standard vacuum line techniques.

2.2. Synthetic Procedure of [Emim][BF$_3$X] Ionic Liquids (General Procedure). A PTFE-lined stainless steel reactor was charged with $[Emim][X]$ (∼10 mmol) and CH_2Cl_2 (∼5 mL) in a dry box. The reactor was cooled to −196 °C and then evacuated for 1 min. The reactor was warmed to −20 to −10 °C, and BF$_3$ gas was introduced into the reactor (∼0.15 MPa). The valve of the reactor should be open during this process to monitor the inside pressure. The introduction of BF$_3$ was repeated several times until the uptake of BF$_3$ gas ceased. The reactor was immersed in an oil bath, and the mixture was stirred for about 16 h. All of the volatiles were roughly pumped off at room temperature for 1 h through a NaOH chemical trap (5 kPa). The final product of $[Emim][BF_3X]$ was obtained by vacuuming at 50–90 °C for 24 h under high vacuum (≤1 Pa) based on the stability of the ILs. The synthetic route and results are shown in Figure 2 and Table 2, respectively.

X= CH$_3$SO$_3$, EtSO$_4$, HSO$_4$, Tos, OTf, NTf$_2$, tfa, Ac, DCA.

Figure 2. Syntheses of $[Emim][BF_3X]$ by acid–base reactions.

2.3. Characterization and Physicochemical Properties of Ionic Liquid. *2.3.1. Characterization.* The structures of $[Emim][BF_3X]$ were confirmed by NMR (^{1}H, ^{13}C, and ^{19}F NMR spectra) and elemental analysis. NMR analyses were performed on a Bruker Advance 500 spectrometer using acetonitrile as the internal standard solvent. Proton shifts were reported in δ units downfield from Me$_4$Si with the solvent as the reference signal, and hexafluorobenzene was used as a reference for the ^{19}F NMR spectra. Carbon, hydrogen, nitrogen, and sulfur contents were determined using an elemental analyzer (Vario EL Cube).

2.3.2. Phase Transitions. The melting point and glass-transition temperature were determined using DSC (Netzsch DSC 214 Polyma). All samples were weighed in aluminum pans, and these sealed pans were heated in a nitrogen atmosphere from 20 to 60 °C before cooling to −150 °C and reheating again to 60 °C. The glass-transition temperature (T_g, onset of the heat capacity change), crystallization temperature

Table 1. List of Chemicals, Abbreviation, Supplier, Purity, and Water Content

chemical name	abbreviation	source	purity[a] (%)	water content after drying (ppm)
1-ethyl-3-methylimidazolium methanesulfonate	$[Emim][CH_3SO_3]$	Alfa Aesar	≥99	210
1-ethyl-3-methylimidazolium ethylsulfate	$[Emim][EtSO_4]$	TCI	≥98	220
1-ethyl-3-methylimidazolium hydrogen sulfate	$[Emim][HSO_4]$	Macklin	≥98	240
1-ethyl-3-methylimidazolium trifluoromethanesulfonate	$[Emim][OTf]$	TCI	≥98	168
1-ethyl-3-methylimidazolium tosylate	$[Emim][Tos]$	Macklin	≥98	350
1-ethyl-3-methylimidazolium bis[(trifluoromethyl)sulfonyl]imide	$[Emim][NTf_2]$	Sigma-Aldrich	≥98	215
1-ethyl-3-methylimidazolium dicyanamide	$[Emim][DCA]$	Alfa Aesar	≥99	216
1-ethyl-3-methylimidazolium trifluoroacetate	$[Emim][tfa]$	Sigma-Aldrich	≥98	166
1-ethyl-3-methylimidazolium acetate	$[Emim][Ac]$	Sigma-Aldrich	≥98	247
1-ethyl-3-methylimidazolium tetrafluoroborate	$[Emim][BF_4]$	Sigma-Aldrich	≥98	196
dichloromethane	DCM	Macklin	≥99.9	1
boron trifluoride	BF$_3$	Shenzhen Jingu Gas	≥99.9	

[a]Purity as mentioned by the supplier.

Table 2. Results of the Synthesis of [Emim][BF₃X]

[Emim][X]	vacuum temperature (°C)	yield^a (%)	product empirical formula from elemental analysis^b	product	water content (ppm)
[Emim][CH₃SO₃]	90	99.2	[Emim][BF₃(CH₃SO₃)]	yellow liquid	323
[Emim][EtSO₄]	70	98.8	[Emim][BF₃(EtSO₄)]	yellow liquid	260
[Emim][HSO₄]	50	98.5	[Emim][BF₃(HSO₄)]	pale yellow liquid	283
[Emim][OTf]	90	82.7	[Emim][(BF₃)₀.₂₅(OTf)]	turbid yellow liquid	
[Emim][Tos]	90	98.9	[Emim][BF₃(Tos)]	yellow liquid	351
[Emim][NTf₂]	90	83.5	[Emim][(BF₃)₀.₀₂(NTf₂)]	pale yellow liquid	
[Emim][DCA]	70	78.4		hard yellow solid	
[Emim][tfa]	70	67.4		turbid yellow liquid	
[Emim][Ac]	70	64.2		turbid yellow liquid	

^{a}The yield was calculated based on crude [Emim][X] and product [Emim][BF₃X]; ^{b}Elemental analysis data could be obtained from the Supporting Information file.

(T_c, onset of the exothermic peak), solid−solid transition temperature (T_{s-s}, onset of the endothermic peak), and melting point (T_m, onset of the endothermic peak), where appropriate, were recorded in the heating/cooling cycle for each IL by heating.

2.3.3. Thermal Stability. The thermal decomposition temperature was measured by using a thermogravimetric analyzer (Netzsch STA 449 F5). An average weight of 5−10 mg for every sample was loaded on a platinum pan and heated at a rate of 10 °C·min⁻¹ over a range of approximately 35−700 °C under a nitrogen atmosphere. The standard uncertainty is $u(T) = \pm 1$ °C. The experimental temperatures of thermal decomposition are presented in terms of weight loss (%) and temperature (°C). The start temperature (T_{start}) is the temperature at which decomposition of the sample begins. The onset temperature (T_{onset}) is the intersection of the baseline weight, from the beginning of the experiment, and the tangent of the weight vs temperature curve as decomposition occurs.

2.3.4. Density and Viscosity. The density and viscosity were measured under open ambient conditions by an Anton Paar Stabinger Viscometer (model SVM 3000) with a temperature range of 293.15−358.15 K This apparatus was calibrated by using Cannon mineral oil in the temperature range from 273.15 to 363.15 K. Standard uncertainties are $u(\rho) = \pm 0.0005$ g·cm⁻³, $u(\eta) = \pm 0.35\%$ mPa·s, and $u(T) = \pm 0.02$ K. All measurements were performed in triplicate, and the average values were reported.

2.3.5. Conductivity. Conductivity was measured by using an LE703 electrode attached to a Mettler Toledo FE30 conductivity meter after calibration with 0.1 M KCl aqueous solution. The temperature was controlled by an external oil bath. The conductivities of ILs were measured under a N₂ atmosphere in a glovebox and each measurement at a specified temperature was completed within 60 min. Standard uncertainties are $u(\sigma) = \pm 0.5\%$ and $u(T) = \pm 0.3$ K. All measurements were performed in triplicate, and the average values were reported.

2.3.6. Surface Tension. Surface tension was measured using a pendant drop method by a KRÜSS DSA25S, and a syringe was used to generate the drop. A camera (Camera CF04) was used to take photographs. Software (Advance) was used to evaluate the shape of the drop. The measurement was recorded in the temperature range of 298.15−343.15 K and under open ambient conditions. The standard uncertainties are $u(T) = \pm 0.1$ K and $u(\gamma) = \pm 1$ mN·m⁻¹. All measurements were performed in triplicate, and the average values were reported.

3. RESULTS AND DISCUSSION

3.1. Synthesis. ILs [Emim][BF₃X] were proposed to be prepared by adding the Lewis acid BF₃ to [Emim][X]. The Lewis acid−base reaction was highly exothermic so that the reactor should be occasionally cooled by a refrigerant. The preparation result of the ILs is influenced by the donicity, basicity, and stability of the anion [X]⁻[23] Low-donicity anions such as [NTf₂]⁻ and [OTf]⁻ were unable to take up the stoichiometry of BF₃. Moderate-donicity anions such as [CH₃SO₃]⁻, [EtSO₄]⁻, [HSO₄]⁻, and [Tos]⁻ could be adopted to prepare the corresponding complex ILs [Emim]-[BF₃X]. However, the strong-donicity anions [DCA]⁻ became hard solid-like stones, while unstable strong-donicity and basic anions, i.e., [tfa]⁻ and [Ac]⁻, reacted with BF₃, resulted in the decomposition of the anion for the strong acid power of BF₃.[24]

3.2. Characterization. Based on elemental analyses and synthetic yields, the synthesized ILs were found to be [Emim][BF₃X] (X= CH₃SO₃, EtSO₄, HSO₄, and Tos). NMR spectroscopy (¹H, ¹³C, and ¹⁹F NMR spectra) of [Emim][BF₃X] showed similar changes compared to [Emim]-[X].

First, there were no significant changes in the chemical shifts and signals for cation [Emim]⁺, while the acidic C-2 hydrogen of the imidazolium cation ring was observed to have an upfield shift of ~0.52 ppm (Table 3), which could be explained by the

Table 3. Chemical Shifts of the Proton at the C (2) Carbon Atom in the Imidazolium Cation for [Emim][BF₃X] and [Emim][X]
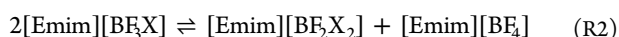
[Emim][BF₃X]	δ(H(2)) (ppm)	[Emim][X]	δ(H(2)) (ppm)
[Emim][BF₃(CH₃SO₃)]	8.51	[Emim][CH₃SO₃]	9.11
[Emim][BF₃(EtSO₄)]	8.46	[Emim][EtSO₄]	8.94
[Emim][BF₃(HSO₄)]	8.50	[Emim][HSO₄]	8.97
[Emim][BF₃(Tos)]	8.49	[Emim][Tos]	9.03
[Emim][BF₄]	9.04		

fact that [BF₃X]⁻ had a relatively weaker basicity than [X]⁻, weakening the interaction between the C-2 hydrogen and the anion.[25] Compared with [BF₄]⁻, the [BF₃X]⁻ anions have weaker interactions with the cationic fragment, so [BF₃X]⁻ is attributed to weakly donating anions.[26]

Second, there were large changes in chemical shifts and signals for the anion after the addition of BF₃ into [X]⁻. Taking [Emim][BF₃(CH₃SO₃)] for instance, after the introduction of BF₃ into [Emim][CH₃SO₃], the resonances of the protons in

$[CH_3SO_3]^-$ split into two lines rather than just a singlet, and the ratio of their integrated signal areas was approximately 3.92:1. Additionally, the ^{13}C NMR spectrum of $[CH_3SO_3]^-$ showed two lines after introducing BF_3 into $[Emim]$-$[CH_3SO_3]$. Finally, the ^{19}F NMR spectrum presented three signals, which were all two overlapping resonances, and the ratio of the integrated signal areas was identical to the isotopic signature of boron (20 ^{10}B, 80% ^{11}B), suggesting the presence of $[BX_4]^-$.[27] The signal at -151.0 ppm corresponded to $[BF_4]^-$ based on the experimental values of $[Emim][BF_4]$, and the signal at -146.82 ppm exhibited the strongest intensity, which could be assigned to the 1:1 adduct $[BF_3(CH_3SO_3)]^-$ with three equivalent fluorine positions. The intensity ratio 1:2 of the signals at -143.30 ppm and -150.1 ppm allowed us to assign the signal at -143.30 ppm to $[BF_2(CH_3SO_3)_2]^-$.[28] Based on ^{19}F NMR integrated signal areas, the ratio of $[BF_3(CH_3SO_3)]^-$ and $[BF_2(CH_3SO_3)_2]^-$ is $(78.2/3)/(7.0/2)$ = 7.45, and this value is approximately equal to the result obtained from ^1H NMR data $((3.92/3)/(1/6) = 7.84)$. Similarly, $[BF_3(EtSO_4)]^-$ and $[BF_3(Tos)]^-$ showed the same NMR phenomenon as $[BF_3(CH_3SO_3)]^-$, with the exception of $[BF_3(HSO_4)]^-$. The proton of $[BF_3(HSO_4)]^-$ was observed as a singlet at 10.01 ppm, which could be explained by the fact that the acidic proton transfer between $[BF_x(HSO_4)_y]^-$ was fast on the NMR time scale. The ^{19}F NMR resonance related to $[BF_3(HSO_4)]^-$ showed four distinct resonances with broader and more complicated signals, possibly due to quick disproportionation and redistribution of the ligands in $[BF_3(HSO_4)]^-$.

The analysis of NMR data showed that complexing of BF_3 with $[Emim][X]$ was prone to disproportionation and redistribution of the ligands in $[BF_3X]^-$,[29] and the disproportionation of $[BF_3X]$ proceeded by way of reactions R1 to (RR2)

$$BF_3 + [Emim][X] \rightleftharpoons [Emim][BF_3X] \quad (R1)$$

$$2[Emim][BF_3X] \rightleftharpoons [Emim][BF_2X_2] + [Emim][BF_4] \quad (R2)$$

The extent of disproportionation of $[BF_3X]^-$ and equilibrium constants for reaction R2 (K_2) are listed in Table 4.

Table 4. Extent of Disproportionation of $[BF_3X]^-$

X	$[BF_3X]^-$ (%)	$[BF_2X_2]^-$ (%)	$[BF_4]^-$ (%)	K_2
CH_3SO_3	78.4	10.5	11.1	0.019
$EtSO_4$	84.7	7.7	7.7	0.0082
Tos	82.6	8.7	8.7	0.011

Considering that the content of $[Emim][BF_3X]$ is ~80% and that the majority of ILs mixtures exhibit close to ideal mixing behavior, it could be assumed that the formula $[Emim][BF_3X]$ could represent the synthesized ILs.[30]

3.3. Phase Transitions. The solid−liquid phase transition of $[Emim][BF_3X]$ was studied by differential scanning calorimetry (DSC). DSC curves are listed in the Supporting Information (Figures S21−S24), and the obtained values for these ILs are shown in Table 5. The results showed that there were no melting or freezing points but only glass-transition temperatures (T_g). These ILs have no true phase transitions but only the formation of an amorphous glass on cooling and reformation of the liquid on heating. T_g reflects the total cohesive energy within the liquid salt, and it is related to the separation between the ions.[1] The T_g of $[Emim][BF_3X]$ is

Table 5. T_g of $[Emim][BF_3X]$ Obtained by DSC Analysis

$[Emim][BF_3X]$	T_g (°C)	$[Emim][X]$	T_g (lit.) (°C)
$[Emim][BF_3(CH_3SO_3)]$	−86.53	$[Emim][CH_3SO_3]$	−60.95[32]
$[Emim][BF_3(EtSO_4)]$	−99.86	$[Emim][EtSO_4]$	−80.25[33]
$[Emim][BF_3(HSO_4)]$	−93.36	$[Emim][HSO_4]$	−63.05[33]
$[Emim][BF_3(Tos)]$	−65.58	$[Emim][Tos]$	−39.15[33]
$[Emim][BF_4]$	−92.6[34]		

lower than that of the corresponding $[Emim][X]$, which could explain that ILs with large charge-diffuse ions have lower T_g values compared to those with more localized charges despite larger molar volumes. The T_g values increase in the order $[Emim][BF_3(EtSO_4)]$ < $[Emim][BF_3(HSO_4)]$ < $[Emim]$-$[BF_4]$ < $[Emim][BF_3(CH_3SO_3)]$ < $[Emim][BF_3(Tos)]$, and this sequence is consistent with the trend in T_g values for $[Emim][X]$. $[Emim][BF_3(Tos)]$ has the highest T_g value compared to other $[Emim][BF_3X]$, which could be interpreted that the increase in ion size increases the van der Waals force, which is predominant over its high charge distribution.[31]

3.4. Thermal Stability. Thermogravimetric analysis (TGA) curves are given in Figures 3 and S25. Table 6 shows the onset and start temperatures for $[Emim][BF_3X]$ as well as comparisons with $[Emim][X]$. The T_{start} (73.4−141.8 °C) and T_{onset} (322.0−334.8 °C) values for the $[Emim][BF_3X]$ are much lower than those for $[Emim][BF_4]$ (T_{onset} = 443 °C)[35] and $[Emim][X]$, which is essentially attributed to the thermal lability of the $[BF_3X]^-$, plausibly corresponding to the release of BF_3. The thermal stability of $[Emim][BF_3X]$ decreases in the order $[Emim][BF_3(Tos)]$ > $[BF_3(CH_3SO_3)]$ ≫ $[Emim][BF_3(HSO_4)]$ > $[Emim][BF_3(EtSO_4)]$. $[Emim]$-$[BF_3(HSO_4)]$ showed low thermal stability due to the weak intermolecular force of $[HSO_4]^-$ with BF_3. $[Emim]$-$[BF_3(EtSO_4)]$ revealed the lowest thermal stability, which is related to the lowest thermal stability of the $[EtSO_4]^-$ anion.

3.5. Density. Density is an important physicochemical property in the design of many technological processes. The measured density values for the ILs are listed in Tables 7, S1, and Figure 4. The densities of the $[Emim][BF_3X]$ ILs increase by 5.04−8.97% compared to the corresponding $[Emim][X]$, which could be attributed to the heavier molecular weight of the anion. The density values decreased in the following sequence: $[Emim][BF_3(HSO_4)]$ > $[Emim][BF_3(CH_3SO_3)]$ > $[Emim][BF_3(EtSO_4)]$ > $[Emim][BF_3(Tos)]$ > $[Emim][BF_4]$, and this sequence is consistent with the trend in density values for $[Emim][X]$. These results indicate that the densities are not only related to the anion molecular weight but also related to the interactions between cations and anions. $[Emim]$-$[BF_3(HSO_4)]$ shows the highest density value, even though the molecular mass of its anion is relatively small, which could be ascribed to strong molecular force and hydrogen bonding in the presence of anion.

The temperature dependence of the density data was fitted by a simple linear regression (eq 1)

$$\rho = A_0 + A_1 T \quad (1)$$

where A_0 and A_1 are fitting parameters, T is the Kelvin temperature in K, and ρ is the density in g·cm^{-3}. The respective values of the correlation coefficients for all of the ILs are listed in Table 8, together with the correlation coefficients (R^2) and the standard deviations (SD), which was calculated using eq 2
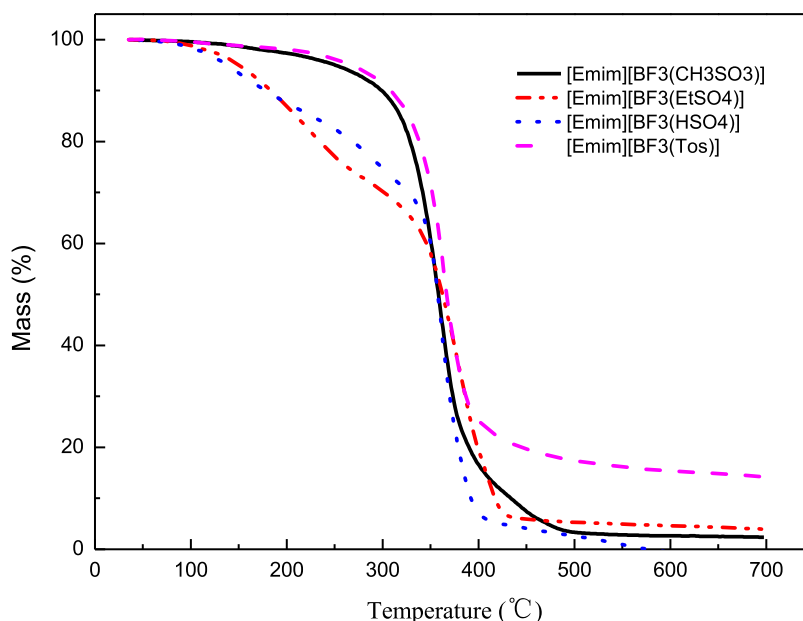
Figure 3. Thermogravimetric analysis (TGA) curves of [Emim][BF$_3$X].

Table 6. T_{start} and T_{onset} of [Emim][BF$_3$X] and [Emim][X] Obtained by TGA

[Emim][BF$_3$X]	T_{start} (°C)	T_{onset} (°C)	[Emim][X]	T_{start} (°C)	T_{onset} (°C)
[Emim][BF$_3$(CH$_3$SO$_3$)]	130.5	326.2	[Emim][CH$_3$SO$_3$]	284.3	349.7
[Emim][BF$_3$(EtSO$_4$)]	73.4	300.8	[Emim][EtSO$_4$]	165.4	347.7
[Emim][BF$_3$(HSO$_4$)]	88.9	322	[Emim][HSO$_4$]	294.5	362.7
[Emim][BF$_3$(Tos)]	141.8	334.8	[Emim][Tos]	251.2	341.7

$$SD = \sqrt{\frac{\sum (Z_{exp} - Z_{cal})^2}{n}} \qquad (2)$$

where Z_{exp} is the experimental value, Z_{cal} is the calculated value, and n is the number of experimental points.

The measured values of density were then used to calculate some important volumetric properties, including the isobaric thermal expansion coefficients α_ρ, the molecular volume V_m, the standard entropy S^0, and the lattice potential energy U_{POT}.[36]

3.5.1. Isobaric Thermal Expansion Coefficient.
The isobaric thermal expansion coefficient (α_ρ) of each IL was calculated using eq 3

$$\alpha_\rho = -\frac{1}{\rho}\left(\frac{\partial \rho}{\partial T}\right)_p = -\frac{A_1}{A_0 + A_1 T} \qquad (3)$$

where p is the pressure in MPa.

The α_ρ values of all studied ILs are presented in Table 9 for the temperatures of 298.15 and 358.15 K. Table 9 shows that the thermal expansion coefficients of [Emim][BF$_3$X] do not noticeably change within the temperature range of 298.15−358.15 K. The average relative deviation of α_ρ is less than 4%. This implies that these ILs almost have a temperature independency of the thermal expansion coefficient from α_ρ= 5.1922 × 10^{-4} to 6.0614 × 10^{-4} K^{-1}, and this behavior was compatible with [Emim][BF$_4$] and [Emim][X].[37] For the selected temperature, the α_ρ values follow the IL anion sequence [BF$_4$]$^-$ > [BF$_3$(EtSO$_4$)]$^-$ > [BF$_3$(CH$_3$SO$_3$)]$^-$ > [BF$_3$(Tos)]$^-$ > [BF$_3$(HSO$_4$)]$^-$, and the α_ρ values of [Emim]-[BF$_3$X] are greater than those of [Emim][X].

3.5.2. Molecular Volume.
The molecular volume (V_m) of each IL was calculated using eq 4

Table 7. Experimental Values for the Densities (ρ) of the Studied [Emim][BF$_3$X] from 293.15 to 358.15 K at Atmospheric Pressure[a]

temperature (K)	density (g·cm^{-3})				
	[Emim][BF$_3$(CH$_3$SO$_3$)]	[Emim][BF$_3$(EtSO$_4$)]	[Emim][BF$_3$(HSO$_4$)]	[Emim][BF$_3$(Tos)]	[Emim][BF$_4$]
293.15	1.3556	1.3333	1.4378	1.3141	1.2852
298.15	1.3517	1.3297	1.4343	1.3104	1.2810
308.15	1.344	1.3221	1.4267	1.3033	1.2735
318.15	1.3361	1.3141	1.4192	1.2961	1.2663
328.15	1.3282	1.3061	1.4117	1.289	1.2582
338.15	1.3205	1.2986	1.4042	1.2818	1.2510
348.15	1.3128	1.2908	1.3969	1.2746	1.2422
358.15	1.3050	1.2829	1.3896	1.2673	1.2349

[a]Standard uncertainties u are $u(T)$ = 0.02 K and $u(\rho)$ = 0.0005 g·cm^{-3}.
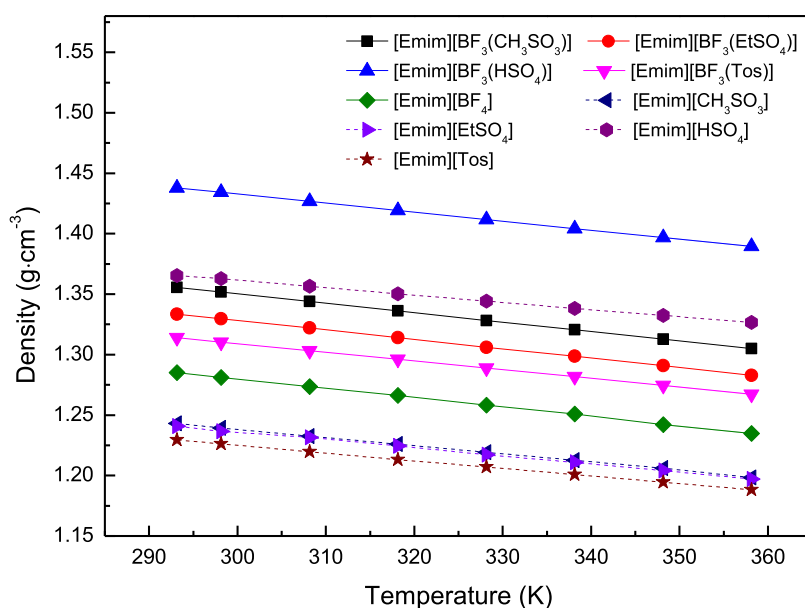
Figure 4. Densities as a function of temperature.

Table 8. Fitting Parameters of Density and Standard Deviations Calculated Using Eq 1

[Emim][BF$_3$X]	A_0	$A_1 \times 10^4$	SD^a	R^2
[Emim][BF$_3$(CH$_3$SO$_3$)]	1.5839	−7.7897	1.04107×10^{-4}	0.99996
[Emim][BF$_3$(EtSO$_4$)]	1.5615	−7.7766	1.54786×10^{-4}	0.99992
[Emim][BF$_3$(HSO$_4$)]	1.6562	−7.4466	1.09999×10^{-4}	0.99995
[Emim][BF$_3$(Tos)]	1.5246	−7.1822	5.76936×10^{-5}	0.99999
[Emim][BF$_4$]	1.5116	−7.7230	3.56601×10^{-4}	0.99956

Table 9. Thermal Expansion Coefficient Values (α_ρ) for [Emim][BF$_3$X] and [Emim][X] at 298.15 K with 358.15 K and Atmospheric Pressure

[Emim][BF$_3$X]	$\alpha_{\rho,298.15} \times 10^4$ (K^{-1})	$\alpha_{\rho,358.15} \times 10^4$ (K^{-1})	[Emim][X]	$\alpha_{\rho,298.15} \times 10^4$ (K^{-1})
[Emim][BF$_3$(CH$_3$SO$_3$)]	5.7631	5.9695	[Emim][CH$_3$SO$_3$]	5.4458
[Emim][BF$_3$(EtSO$_4$)]	5.8486	6.0614	[Emim][EtSO$_4$]	5.4074
[Emim][BF$_3$(HSO$_4$)]	5.1922	5.3592	[Emim][HSO$_4$]	4.4210
[Emim][BF$_3$(Tos)]	5.4806	5.6670	[Emim][Tos]	5.1568
[Emim][BF$_4$]	6.0273	6.2534		

$$V_m = \frac{M}{N_A \rho} \tag{4}$$

where M is the molecular weight in g·mol^{-1}, N_A is Avogadro's number (6.02245×10^{23} molecule mol^{-1}), ρ is the density (g·cm^{-3}) at 298.15 K, and V_m is the molecular volume in nm^3 at 298.15 K.

The V_m values of all studied ILs are presented in Table 10. The V_m values of [Emim][BF$_3$X] increase by ~20.98% compared to the corresponding [Emim][X], which could be attributed to the higher molecular weight of the anion. The V_m values follow the IL anion sequence [BF$_3$(Tos)]$^-$ > [BF$_3$(EtSO$_4$)]$^-$ > [BF$_3$(CH$_3$SO$_3$)]$^-$ > [BF$_3$(HSO$_4$)]$^-$ >

Table 10. Calculated Values of the Volumetric Properties of the ILs at 298.15 K and Atmospheric Pressure

ILs	V_m (nm^3)	S^0 (J·K^{-1}·mol^{-1})	U_{POT} (kJ·mol^{-1})
[Emim][BF$_3$(CH$_3$SO$_3$)]	0.3367	449.2	441.0
[Emim][BF$_3$(EtSO$_4$)]	0.3798	502.8	427.8
[Emim][BF$_3$(HSO$_4$)]	0.3196	427.8	447.0
[Emim][BF$_3$(Tos)]	0.4437	582.6	411.4
[Emim][BF$_4$]	0.2568	349.6	472.9
[Emim][CH$_3$SO$_3$]	0.2761	373.7	464.1
[Emim][EtSO$_4$]	0.3170	424.7	447.9
[Emim][HSO$_4$]	0.2535	345.4	474.5
[Emim][Tos]	0.3821	505.7	427.1

[BF$_4$]$^-$, which is consistent with the molecular weight of the anion.

3.5.3. Standard Molar Entropy. The standard molar entropy (S^0) of each IL was calculated by using eq 5

$$S^\circ(298.15) = 1246.5 \times V_m + 29.5 \tag{5}$$

where S^0 is the standard molar entropy(J·K^{-1}·mol^{-1}) at 298.15 K.

The S^0 values of all of the studied ILs are presented in Table 10. The S^0 values of the [Emim][BF$_3$X] ILs are also notably higher than those of the corresponding [Emim][X], and the result of subtracting the S^0 values of [Emim][BF$_3$X] from [Emim][X] implies entropy contributions of the BF$_3$ group to the entropy for [Emim][BF$_3$X] of about 78.2 J·K^{-1}·mol^{-1}. The S^0 values follow the IL anion sequence [BF$_3$(Tos)]$^-$ > [BF$_3$(EtSO$_4$)]$^-$ > [BF$_3$(CH$_3$SO$_3$)]$^-$ > [BF$_3$(HSO$_4$)]$^-$ > [BF$_4$]$^-$. These phenomena are due to the fact that the large anion size causes little interaction between the cation and the anion, resulting in a higher disordered state and thus a higher standard entropy.
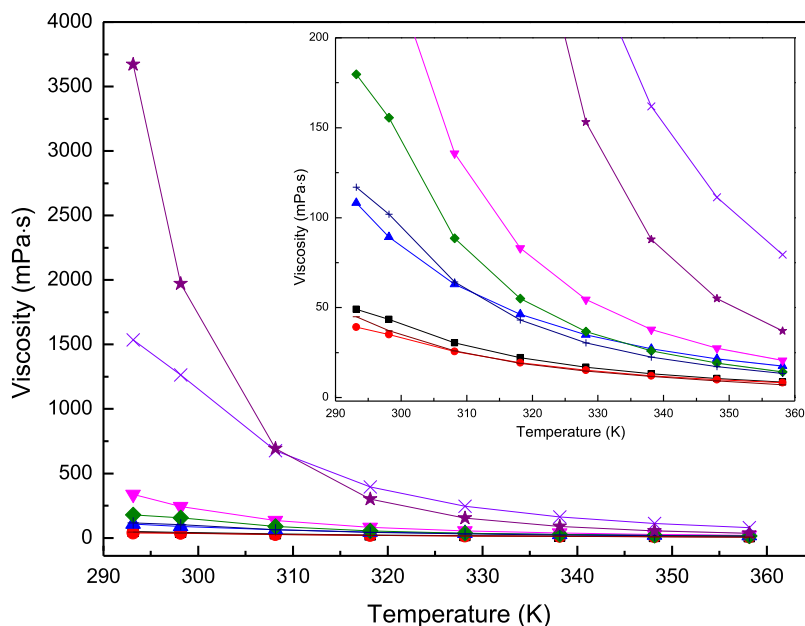
3.5.4. Lattice Potential Energy. The lattice potential energy (U_{POT}) of the synthesized ILs was calculated by using eq 6

$$U_{POT}(298.15) = 1981.2\left(\frac{\rho}{M}\right)^{1/3} + 103.8 \tag{6}$$

Table 11. Experimental Values for the Viscosity (η) of the Studied [Emim][BF$_3$X] from 293.15 to 358.15 K at Atmospheric Pressure[a]

temperature (K)	viscosity (mPa·s)				
	[Emim][BF$_3$(CH$_3$SO$_3$)]	[Emim][BF$_3$(EtSO$_4$)]	[Emim][BF$_3$(HSO$_4$)]	[Emim][BF$_3$(Tos)]	[Emim][BF$_4$]
293.15	49.114	39.202	108.17	337.32	44.924
298.15	43.366	35.059	89.202	242.51	37.112
308.15	30.428	25.593	62.954	135.68	25.935
318.15	22.153	19.385	46.179	83.013	18.926
328.15	16.780	15.139	34.902	54.489	14.752
338.15	13.135	12.129	27.061	37.811	11.763
348.15	10.493	9.926	21.520	27.460	9.3251
358.15	8.515	8.279	17.504	20.703	7.1026

[a]Standard uncertainties u are $u(T)$ = 0.02 K and $u(\eta)$ = 0.35% mPa·s.

Figure 5. Experiment viscosity as a function of temperature: [Emim][BF$_3$(CH$_3$SO$_3$)]:■, [Emim][BF$_3$(EtSO$_4$)]:●, [Emim][BF$_3$(HSO$_4$)]:▲, [Emim][BF$_3$(Tos)]:▼, [Emim][BF$_4$]: —, [Emim][CH$_3$SO$_3$]:◆, [Emim][EtSO$_4$]:+, [Emim][HSO$_4$]:✕, [Emim][Tos]:★.

where U_{POT} is the lattice potential energy (kJ·mol^{-1}) at 298.15 K.

The U_{POT} values of all of the studied ILs are presented in Table 10. The U_{POT} values of the [Emim][BF$_3$X] ILs are also considerably lower than those of [Emim][BF$_4$] and the corresponding [Emim][X]. The U_{POT} values follow the IL anion sequence [BF$_3$(Tos)]$^-$ < [BF$_3$(EtSO$_4$)]$^-$ < [BF$_3$(CH$_3$SO$_3$)]$^-$ < [BF$_3$(HSO$_4$)]$^-$ < [BF$_4$]$^-$, in contrast to the sequence of V_m and S^0. The calculated U_{POT} values for [Emim][BF$_3$X] are 411.4−447.0 kJ·mol^{-1}, much lower than that of cesium iodide lattice energy, which is 613 kJ·mol^{-1}, and this is the lowest value among the alkali halide salts. These low values of lattice potential energy render them as liquids at room temperature.

3.6. Viscosity. Viscosity is a decisive parameter for assessing the use of ILs as media in chemical and electrochemical applications. The viscosity of ILs is relatively high compared with other solvents: at least 10 times higher than water and often significantly greater. This is the result of the strong intermolecular interactions: van der Waals forces, hydrogen bonding, and Coulombic forces. Thus, the low-viscosity ILs are usually composed of low symmetry, low capacity to form hydrogen bonds and charge-delocalized ions.[1,2] For these reasons, [Emim][BF$_3$X] is expected to be less viscous than [Emim][X]. As shown in Table 11, Table S2, and Figure 5, the viscosity of [Emim][BF$_3$X] is approximately 3−14 times lower than that of [Emim][X]. The viscosity of [Emim][BF$_3$X] increases in the anion order of [BF$_3$(EtSO$_4$)]$^-$ ≈ [BF$_4$]$^-$ < [BF$_3$(CH$_3$SO$_3$)]$^-$ ≪ [BF$_3$(HSO$_4$)]$^-$ < [BF$_3$(Tos)]$^-$. The viscosities of [Emim][BF$_3$(EtSO$_4$)] and [Emim][BF$_3$(CH$_3$SO$_3$)] are comparable to that of [Emim]-[BF$_4$], which can be ascribed to the fact that the weaker Coulomb interaction (owing to the improved charge distribution and more conformational degrees of freedom in anions) is overcompensated by the stronger van der Waals interaction (caused by the increased size of [BF$_3$(EtSO$_4$)]$^-$ versus [BF$_4$] ions). [Emim][BF$_3$(HSO$_4$)] has a high viscosity, which is attributed to the formation of hydrogen bonds between the hydrogen atoms and the fluorine atom or oxygen atom at the anion, while the highest viscosity for [Emim]-[BF$_3$(Tos)] suggests that the van der Waals interaction has taken over the Coulomb forces to govern the viscosity.

The Arrhenius equation, as described in eq 7, was used to correlate the experimental viscosity data
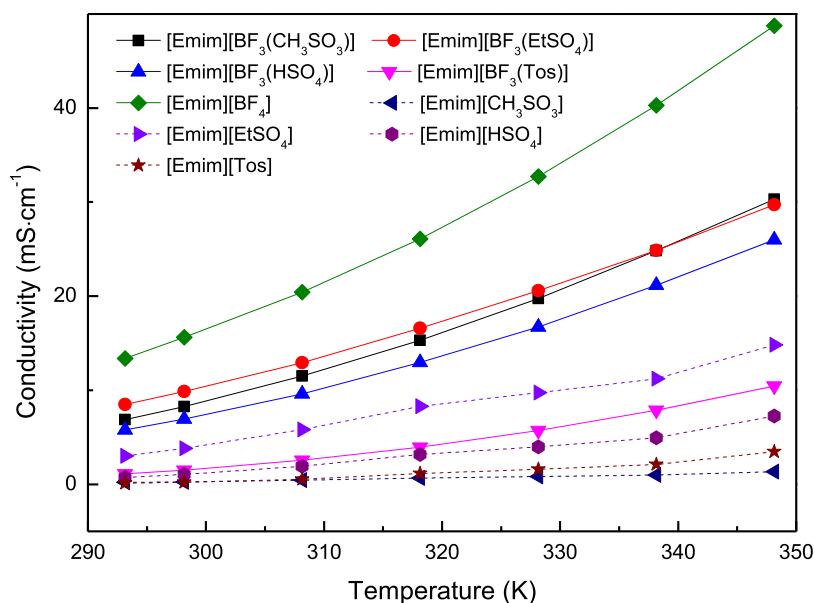
$$\ln \eta = A_2 + A_3/T \tag{7}$$

Table 12. Fitting Parameters of Viscosity, Standard Deviations Calculated Using Eq 7, and the Viscosity Activation Energy ($E_{a,\eta}$) Calculated Using Eq 8

[Emim][BF$_3$X]	A_2	A_3	SD	R^2	$E_{a,\eta}$ (kJ·mol^{-1})
[Emim][BF$_3$(CH$_3$SO$_3$)]	−5.9393	2882.5	0.02626	0.99813	23.97
[Emim][BF$_3$(EtSO$_4$)]	−5.0643	2560.1	0.02208	0.99832	21.28
[Emim][BF$_3$(HSO$_4$)]	−5.4023	2945.9	0.02736	0.99805	24.49
[Emim][BF$_3$(Tos)]	−9.6760	4509.7	0.08399	0.99222	37.49
[Emim][BF$_4$]	−6.1744	2913.8	0.03265	0.99717	24.23

Table 13. Experimental Values for the Conductivity (σ) of the Studied [Emim][BF$_3$X] from 293.15 to 348.15 K at Atmospheric Pressure[a]

	conductivity (mS·cm^{-1})				
temperature (K)	[Emim][BF$_3$(CH$_3$SO$_3$)]	[Emim][BF$_3$(EtSO$_4$)]	[Emim][BF$_3$(HSO$_4$)]	[Emim][BF$_3$(Tos)]	[Emim][BF$_4$]
293.15	6.871	8.483	5.769	1.113	13.37
298.15	8.252	9.86	6.932	1.515	15.63
308.15	11.51	12.94	9.62	2.559	20.41
318.15	15.31	16.59	12.97	3.941	26.1
328.15	19.74	20.58	16.72	5.732	32.72
338.15	24.83	24.88	21.15	7.881	40.27
348.15	30.29	29.74	25.99	10.44	48.76

[a]Standard uncertainties u are $u(T)$ = 0.3 K and $u(\sigma)$ = 0.5% mS·cm^{-1}.

Figure 6. Experiment conductivity as a function of temperature.

where A_2 and A_3 are fitting parameters, T is the Kelvin temperature in K, and η is the viscosity in mPa·s. The fitting parameters, the standard deviations (SD), and the correlation coefficients (R^2) are shown in Table 11.

The viscosity activation energy ($E_{a,\eta}$, kJ·mol^{-1}) of each IL was calculated using eq 8

$$E_{a,\eta} = A_3R/1000 \qquad (8)$$

where R is the gas constant (8.314 J·mol^{-1}·K^{-1}).

The $E_{a,\eta}$ values of all studied ILs are presented in Tables 12 and S3. Theoretically, $E_{a,\eta}$ can be represented as the energy barrier to be overcome by mass transfer, and a more viscous fluid tends to possess a higher $E_{a,\eta}$ value.[38] The $E_{a,\eta}$ of [Emim][BF$_3$X] increases in the anion order of [BF$_3$(EtSO$_4$)]$^-$ < [BF$_3$(CH$_3$SO$_3$)]$^-$ < [BF$_4$]$^-$ < [BF$_3$(HSO$_4$)]$^-$ < [BF$_3$(Tos)]$^-$, and the $E_{a,\eta}$ values of [Emim][BF$_3$X] are lower

than that of [Emim][X] (Table S3). These experimental results are consistent with theory analysis.

3.7. Conductivity. Ionic conductivity is one of the most important properties of ILs as electrolytes. ILs present reasonably good ionic conductivities compared with those of organic solvents/electrolyte systems (up to 20 mS·cm^{-1}). Generally, the conductivity of an IL is primarily governed by its viscosity and ion sizes: the viscosity is exactly opposite to that of conductivity. When the ILs have comparable viscosities, small ions are favorable for the production of highly conductive ILs.[1,39] As shown in Tables 13 and S4 and Figure 6, the conductivity of [Emim][BF$_3$X] is increased by approximately 2.5−32 times compared to [Emim][X], which could be attributed to the lower viscosity (reduced by approximately 3−14 times) of [Emim][BF$_3$X] versus [Emim][X]. The conductivity of [Emim][BF$_3$X] decreases in the anion order

Table 14. Fitting Parameters of Conductivity Calculated Using Eq 9

Emim][BF₃X]	σ_0 (mS·cm⁻¹)	A4 (K)	$T_{0,\sigma}$ (K)	SD	R^2
[Emim][BF₃(CH₃SO₃)]	1034.50	655.77	162.40	0.04493	0.99997
[Emim][BF₃(EtSO₄)]	926.04	707.95	142.30	0.05212	0.99995
[Emim][BF₃(HSO₄)]	1261.21	763.54	151.45	0.03201	0.99998
[Emim][BF₃(Tos)]	594.72	625.47	193.44	0.00893	0.99999
[Emim][BF₄]	5108.8	1179.63	94.57	0.04866	0.99998

Table 15. Surface Tension (γ) Experimental Values from 298.15 to 343.15 K at Atmospheric Pressure[a]

temperature (K)	surface tension (mN·m⁻¹)				
	[Emim][BF₃(CH₃SO₃)]	[Emim][BF₃(EtSO₄)]	[Emim][BF₃(HSO₄)]	[Emim][BF₃(Tos)]	[Emim][BF₄]
298.15	51.93	46.57	57.15	48.80	54.85
303.15	51.59	46.16	56.75	48.58	54.48
313.15	51.15	45.65	55.70	48.22	53.75
323.15	50.36	45.12	54.78	47.61	53.02
333.15	49.95	44.25	54.03	47.24	52.29
343.15	49.26	43.57	52.97	46.74	51.56

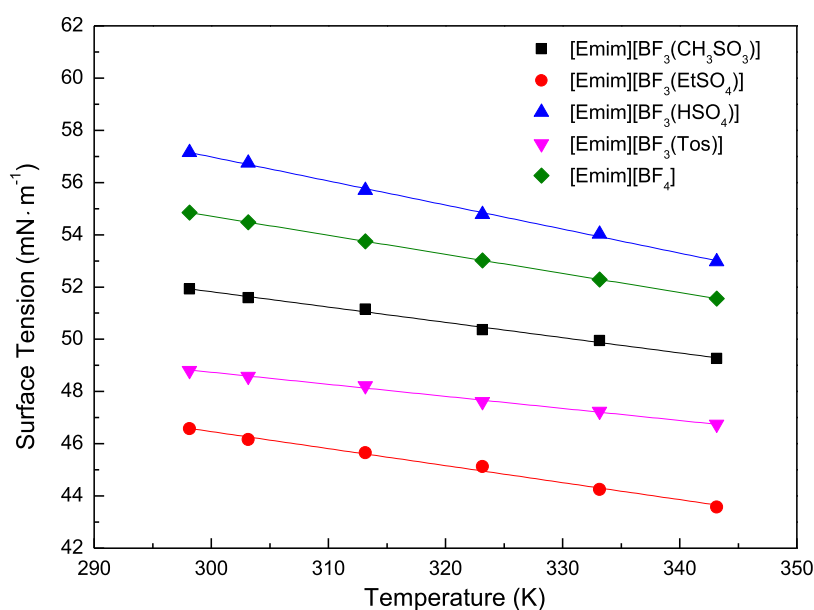[a]Standard uncertainties u are $u(T) = 0.1$ K and $u(\gamma) = 1$ mN·m⁻¹.

Figure 7. Surface tension of the present ILs versus temperature.

of $[BF_4]^- > [BF_3(EtSO_4)]^- > [BF_3(CH_3SO_3)]^- > [BF_3(HSO_4)]^- > [BF_3(Tos)]^-$. This trend can be regarded as the combined result of the viscosity and ion size. Therefore, $[Emim][BF_4]$ shows the highest conductivity, mainly owing to its low viscosity and the lowest formula weight of the anion. $[Emim][BF_3(CH_3SO_3)]$ and $[Emim][BF_3(CH_3SO_3)]$ display higher conductivity values than $[Emim][BF_3(HSO_4)]$ due to their lower viscosity despite their heavier anion weight, while $[Emim][BF_3(Tos)]$ has the lowest conductivity due to its highest viscosity and heaviest formula weight of the anion.

The Vogel–Tammann–Fulcher (VTF) equation (eq 9) was used to represent the temperature dependence of conductivity.

$$\sigma = \sigma_0 \exp\left(\frac{-A_4}{(T - T_{0,\sigma})}\right)$$

(9)

where σ_0 is the ionic conductivity at infinite temperature (mS·cm⁻¹), A_4 is fitting parameter (K), $T_{0,\sigma}$ and T are temperatures in K, and σ is the conductivity in mS·cm⁻¹. The best-fitting

parameters, standard deviations (SD), and correlation coefficients (R^2) are shown in Table 14. The values of the R^2 are >0.9999 and the SD are about 0.03733 for the studied ILs.

3.8. Surface Tension. The surface tension γ is an important property of all liquids, including ILs. Very broadly, the surface tension of ILs falls in the region between 30 and 60 mN·m⁻¹. The surface tensions of $[Emim][BF_3X]$ ILs were measured at atmospheric pressure in the temperature range 298.15–343.15 K and are given in Table 15 and Figure 7. It shows an inverse linear relationship with increasing temperature and decreases in the order of $[Emim][BF_3(HSO_4)] > [Emim][BF_4] > [Emim][BF_3(CH_3SO_3)] > [Emim]-[BF_3(Tos)] > [Emim][BF_3(EtSO_4)]$. It is noted that $[Emim]-[BF_3(HSO_4)]$ exhibits the highest surface tension value, which is attributed to the formation of intermolecular H-bonds. Other $[Emim][BF_3X]$ with lower surface tension values than $[Emim][BF_4]$, such as $[Emim][n\text{-}C_nH_{2n+1}BF_3]$ $(n = 1-5)$, show a tendency for long alkyl chains and hydrophobic groups

to produce low surface tensions due to the low cohesive energy of such liquids.[40]

The surface thermodynamic properties, namely, the surface entropy and the surface enthalpy, were derived by using the quasilinear dependence of the surface tension with temperature (eq 10)

$$\gamma = A_5 - A_6 T \qquad (10)$$

where the intercept A_5 of eq 9 can be identified as the surface enthalpy H^γ (mJ·m^{-2}) and the slope A_6 as the surface entropy S^γ (mJ·m^{-2}·K^{-1}). The values of H^γ, S^γ, standard deviations (SD), and regression coefficient (R^2) are presented in Table 16. It is noted that [Emim][BF$_3$(HSO$_4$)] has the highest

Table 16. Surface Thermodynamic Functions (H^γ, S^γ) of the Studied ILs

[Emim][BF$_3$X]	H^γ (mJ·m^{-2})	S^γ (mJ·m^{-2}·K^{-1})	SD	R^2
[Emim][BF$_3$(CH$_3$SO$_3$)]	69.41	0.059	0.064509	0.99435
[Emim][BF$_3$(EtSO$_4$)]	66.01	0.065	0.085398	0.99122
[Emim][BF$_3$(HSO$_4$)]	84.62	0.092	0.060202	0.99824
[Emim][BF$_3$(Tos)]	62.59	0.046	0.044785	0.99537
[Emim][BF$_4$]	76.63	0.073	0.002155	0.99921

values of surface entropy and surface enthalpy, similar to other protic ILs, indicating less surface organization as well as a less structured liquid phase. Other [Emim][BF$_3$X] ILs exhibit a trend that the surface entropies and surface enthalpies decrease with increasing anion size.[41]

3.9. Ionicity. The effective way to evaluate the ionicity of ILs is to adopt the Walden rule to compare molar conductivities (Λ) at similar viscosities and to use the "Walden Plot" of log Λ versus log ($1/\eta$) and compare with reference data obtained from dilute aqueous KCl solutions. As the dilute aqueous KCl solutions contain similarly sized, largely independent mobile ions, the ionicity of KCl approaches 1

in this case, providing a good point of reference on such a plot.[1]

The values of density and conductivity were used to calculate the molar conductivity using eq 11

$$\Lambda = \sigma M / \rho \qquad (11)$$

where Λ represents molar conductivity (S·cm^2·mol^{-1}).

The relationship between the molar conductivity and viscosity can be described by the Walden rule (eq 12).

$$\Lambda \eta = W \qquad (12)$$

where W represents a temperature-dependent constant.

Figure 8 shows the Walden plots for these ILs at different temperatures from 293.15 to 343.15 K. The plots approaching straight lines indicate that all [Emim][BF$_3$X] ILs in this work conform to the Walden rule. In fact, they are significantly closer to the ideal line with unit slope. [Emim][BF$_3$(HSO$_4$)] lies in the upper part of the Walden diagram, which means that it is a super ionic liquid in which the Grothus mechanism for the transport of protons becomes predominant.[42] Other [Emim][BF$_3$X] ILs curves are closely under the ideal KCl line, such as [Emim][BF$_4$], so the [Emim][BF$_3$X] ILs are considered "good ionic liquids".[43]

4. CONCLUSIONS

Four new complex anion ILs [Emim][BF$_3$X] (X = CH$_3$SO$_3$, EtSO$_4$, HSO$_4$, and Tos) were synthesized and characterized. Several equilibria among the anionic species [BF$_3$X]$^-$, [BF$_2$X$_2$]$^-$, and [BF$_4$]$^-$ are assumed to take place in [Emim][BF$_3$X], in which the [BF$_3$X]$^-$ anion is the most abundant anionic species. The [BF$_3$X]$^-$ anions have weaker interactions with the cationic fragments compared with [X]$^-$, based on the chemical shift for the proton at the C(2) atom of the imidazolium cation ring. Thermal characterization results revealed that [Emim][BF$_3$X] have no melting or freezing points but only glass-transition temperatures and the thermal decomposition temperatures (T_{onset}) ranging from 300.8 to 334.8 °C. [Emim][BF$_3$X] possesses visibly higher density, lower viscosity, and higher ionic conductivity than that of the
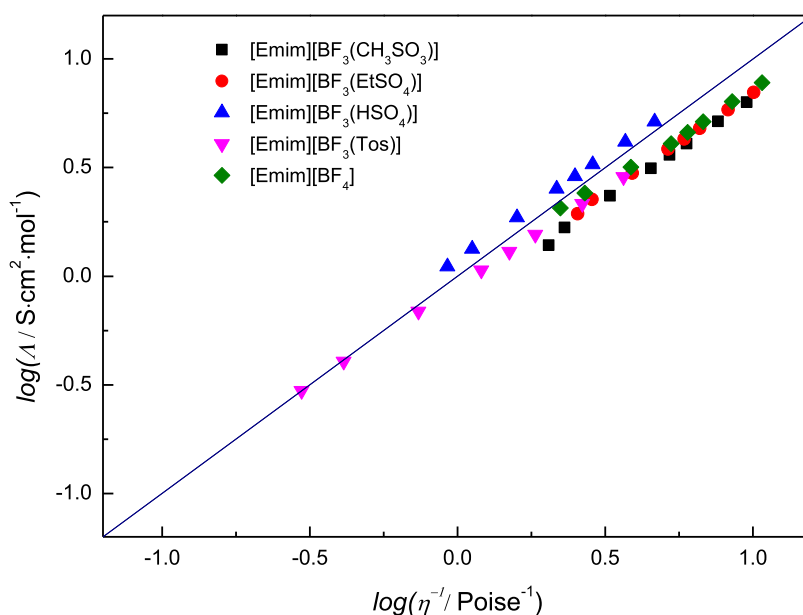
Figure 8. Walden plots for the [Emim][BF$_3$X] ILs.

corresponding [Emim][X]. Compared with [Emim][X], [Emim][BF$_3$X] has higher isobaric thermal expansion coefficient, molecular volume, standard molar entropy, lower lattice potential energy, and viscosity activation energy. The resulting physical properties show that the effect of anion identity is predominant. The Walden rule analysis demonstrates that these ILs comply with the Walden rule well, and they are classified as "good (or super) ionic liquids". Based on the characterization and physicochemical properties of the [Emim][BF$_3$X], we can conclude that complexing BF$_3$ with [Emim][X] would reduce the interaction between the cationic and anionic fragments, obtain an asymmetric, highly flexible, and charge-delocalized anion, and allow us to effectively tune these properties of [Emim][X]. Furthermore, the tuning of application properties such as acidity, alkalinity, hydrophobicity, gas solubility, and many others by hybrid complexation of Lewis fluoroacids BF$_3$ with common ILs will be reported in subsequent studies.

ASSOCIATED CONTENT

Ⓢ Supporting Information

The Supporting Information is available free of charge at https://pubs.acs.org/doi/10.1021/acsomega.3c05697.

Characterization (^{1}H, ^{13}C, ^{19}F NMR spectra, elemental analysis) and DSC analysis for all studied ILs and several physical properties of [Emim][X], including density, viscosity, and conductivity (PDF)

AUTHOR INFORMATION

Corresponding Authors

Wei Zhang — *State Key Laboratory of Fluorine & Nitrogen Chemicals, Xi'an Modern Chemistry Research Institute, Xi'an 710065, China*; Phone: 86-029-88291213; Email: Zhangwei_204@163.com

Jian Lu — *State Key Laboratory of Fluorine & Nitrogen Chemicals, Xi'an Modern Chemistry Research Institute, Xi'an 710065, China*; ⓞ orcid.org/0000-0002-0494-2498; Email: lujian204@263.net

Authors

Ji-Jun Zeng — *State Key Laboratory of Fluorine & Nitrogen Chemicals, Xi'an Modern Chemistry Research Institute, Xi'an 710065, China*; ⓞ orcid.org/0000-0003-4426-2021

Bo Zhao — *State Key Laboratory of Fluorine & Nitrogen Chemicals, Xi'an Modern Chemistry Research Institute, Xi'an 710065, China*; ⓞ orcid.org/0000-0003-1346-5846

Yu An — *State Key Laboratory of Fluorine & Nitrogen Chemicals, Xi'an Modern Chemistry Research Institute, Xi'an 710065, China*

Xiao-Bo Tang — *State Key Laboratory of Fluorine & Nitrogen Chemicals, Xi'an Modern Chemistry Research Institute, Xi'an 710065, China*

Sheng Han — *State Key Laboratory of Fluorine & Nitrogen Chemicals, Xi'an Modern Chemistry Research Institute, Xi'an 710065, China*

Zhi-Qiang Yang — *State Key Laboratory of Fluorine & Nitrogen Chemicals, Xi'an Modern Chemistry Research Institute, Xi'an 710065, China*

Complete contact information is available at:
https://pubs.acs.org/10.1021/acsomega.3c05697

Notes

The authors declare no competing financial interest.

REFERENCES

(1) MacFarlane, D. R.; Kar, M.; Pringle, J. M. *Fundamentals of Ionic Liquids: From Chemistry to Applications*; Wiley-VCH Verlag GmbH & Co. KGaA: Germany, 2017.

(2) *Electrodeposition From Ionic Liquids*; Endres, F.; Abbott, A.; MacFarlane, D., Eds.; Wiley-VCH Verlag GmbH & Co. KGaA: Germany, 2017.

(3) Silva, W.; Zanatta, M.; Ferreira, A. S.; Corvo, M. C.; Cabrita, E. J. Revisiting Ionic Liquid Structure-Property Relationship: A Critical Analysis. *Int. J. Mol. Sci.* **2020**, *21*, 7745−7760.

(4) Philippi, F.; Welton, T. Targeted modifications in ionic liquids—from understanding to design. *Phys. Chem. Chem. Phys.* **2021**, *23*, 6993−7021.

(5) Welton, T. Ionic liquids: a brief history. *Biophys. Rev.* **2018**, *10*, 691−706.

(6) Voroshylova, I. V.; Ferreira, E. S. C.; Malček, M.; Costa, R.; Pereira, C. M.; Cordeiro, M. N. D. S. Influence of the anion on the properties of ionic liquid mixtures: a molecular dynamics study. *Phys. Chem. Chem. Phys.* **2018**, *20*, 14899−14918.

(7) Zhou, Z. B.; Matsumoto, H.; Tatsumi, K. Structure and Properties of New Ionic Liquids Based on Alkyl- and Alkenyltrifluoroborates. *ChemPhysChem* **2005**, *6*, 1324−1332.

(8) Zhou, Z. B.; Matsumoto, H.; Tatsumi, K. Low-Melting, Low-Viscous, Hydrophobic Ionic Liquids: 1-Alkyl(Alkyl Ether)-3-methylimidazolium Perfluoroalkyltrifluoroborate. *Chem. - Eur. J.* **2004**, *10*, 6581−6591.

(9) Snuffin, L. L.; Whaley, L. W.; Yu, L. Catalytic Electrochemical Reduction of CO$_2$ in Ionic Liquid EMIMBF$_3$Cl. *J. Electrochem. Soc.* **2011**, *158*, F155−F158.

(10) Iwasaki, K.; Yoshii, K.; Tsuzuki, S.; Tsuda, T.; Kuwabata, S. Synthesis of Novel Ionic Liquids with Aromatic Trifluoroborate Anions. *ECS Trans.* **2014**, *64*, 83−93.

(11) Landmann, J.; Sprenger, J. A. P.; Hennig, P. T.; Bertermann, R.; Grüne, M.; Würthner, F.; Ignat'ev, Nv.; Finze, M. Perfluoroalkyltricyanoborate and Perfluoroalkylcyanofluoroborate Anions: Building Blocks for Low-Viscosity Ionic Liquids. *Chem. - Eur. J.* **2018**, *24*, 608−623.

(12) Ignat'ev, N.V.; Welz-Biermann, U.; Kucheryna, A.; Bissky, G.; Willner, H. New Ionic Liquids with Tris(perfluoroalkyl)trifluorophosphate (FAP) Anions. *J. Fluorine Chem.* **2005**, *36*, 1150−1159.

(13) Bejan, D.; Ignat'ev, N.; Willner, H. New ionic liquids with the bis[bis(pentafluoroethyl)phosphinyl]imide anion, [(C$_2$F$_5$)$_2$P-(O)]$_2$N$^-$—Synthesis and characterization. *J. Fluorine Chem.* **2010**, *131*, 325−332.

(14) Johansson, K. M.; Adebahr, J.; Howlett, P. C.; Forsyth, M.; Macfarlane, D. R. N-methyl-N-alkylpyrrolidinium bis-(perfluoroethylsulfonyl)amide ([NPf$_2$]$^-$) and tris-(trifluoromethanesulfonyl)methide ([CTf$_3$]$^-$) salts: Synthesis and characterization. *Aust. J. Chem.* **2007**, *60*, 57−63.

(15) Liu, K.; Zhou, Y.-X.; Han, H.-B.; Zhou, S.-S.; Feng, W.-F.; Nie, J.; Li, H.; Huang, X.-J.; Armand, M.; Zhou, Z.-B. Ionic liquids based on (fluorosulfonyl)(pentafluoroethanesulfonyl)imide with various oniums. *Electrochim. Acta* **2010**, *55*, 7145−7151.

(16) Prikhod'ko, S. A.; Shabalin, A. Y.; Shmakov, M. M.; Bardin, V.V.; Adonin, N. Y. Ionic liquids with fluorine-containing anions as a new class of functional materials: features of the synthesis, physicochemical properties, and use. *Russ. Chem. Bull.* **2020**, *69*, 17−31.

(17) Herath, M. B.; Creager, S. E.; Kitaygorodskiy, A.; DesMarteau, D. D. Effect of Perfluoroalkyl Chain Length on Proton Conduction in Fluoroalkylated Phosphonic, Phosphinic, and Sulfonic Acids. *J. Phys. Chem. B* **2010**, *114*, 14972−14976.

(18) Adonin, N. Y.; Prikhod'ko, S. A.; Bardin, V.V.; Parmon, V. N. The first example of the ortho-directing effect of the weakly coordinating substituent [−BF₃]⁻ in the catalytic hydrodefluorination of the pentafluorophenyltrifluoroborate anion. *Mendeleev Commun.* **2009**, *19*, 260−262.

(19) Bardin, V. V.; Adonin, N. Y.; Frohn, H.-J. (Fluoroorgano)-fluoroboranes and -borates. 14. Preparation of Potassium ((Perfluoroorgano)ethynyl)trifluoroborates K[R_FC⫶CBF₃]. *Organometallics* **2005**, *24*, 5311−5317.

(20) Eiden, P.; Krossing, I. 'Unusual Anions' as Ionic Liquid Constituents. In *Ionic Liquids Completely UnCOILed*; John Wiley & Sons, Inc.: NJ, 2015; pp 39−54.

(21) Matsumoto, K.; Hagiwara, R.; Yoshida, R.; Ito, Y.; Mazej, Z.; Benkič, P.; Žemva, B.; Tamada, O.; Yoshino, H.; Matsubara, S. Syntheses, structures and properties of 1-ethyl-3-methylimidazolium salts of fluorocomplex anions. *Dalton Trans.* **2004**, *1*, 144−149.

(22) Singh, S. K.; Savoy, A. W. Ionic liquids synthesis and applications: An overview. *J. Mol. Liq.* **2020**, *297*, 112038−112061.

(23) Schmeisser, M.; Illner, P.; Puchta, R.; Zahl, A.; van Eldik, R. Gutmann Donor and Acceptor Numbers for Ionic Liquids. *Chem. - Eur. J.* **2012**, *18*, 10969−10982.

(24) McNeice, P.; Marr, P. C.; Marr, A. C. Basic ionic liquids for catalysis: the road to greater stability. *Catal. Sci. Technol.* **2021**, *11*, 726−741.

(25) Cha, S.; Ao, M.; Sung, W.; Moon, B.; Ahlström, B.; Johansson, P.; Ouchi, Y.; Kim, D. Structures of ionic liquid−water mixtures investigated by IR and NMR spectroscopy. *Phys. Chem. Chem. Phys.* **2014**, *16*, 9591−9601.

(26) Bankmann, D.; Giernoth, R. Magnetic resonance spectroscopy in ionic liquids. *Prog. Nucl. Magn. Reson. Spectrosc.* **2007**, *51*, 63−90, DOI: 10.1016/j.pnmrs.2007.02.007.

(27) Wiemers-Meyer, S.; Winter, M.; Nowak, S. Mechanistic insights into lithium ion battery electrolyte degradation − a quantitative NMR study. *Phys. Chem. Chem. Phys.* **2016**, *18*, 26595−26601.

(28) Brownstein, S.; Latremouille, G. Complex fluoroanions in solution. IX. BF₃-anion complexes and their disproportionation. *Can. J. Chem.* **1978**, *56*, 2764−2767.

(29) Glavincevski, B.; Brownstein, S. Complexing, exchange and reactions of tungsten hexafluoride with some simple anions. *J. Inorg. Nucl. Chem.* **1981**, *43*, 1827−1829.

(30) Stark, A.; Wild, M.; Ramzan, M.; Azim, M. M.; Schmidt, A. *Product Design and Engineering: Formulation of Gels and Pastes*; Wiley-VCH Verlag GmbH & Co. KGaA: Germany, 2013; pp 182−190.

(31) Zhou, Z.-B.; Matsumoto, H.; Tatsumi, K. Cyclic Quaternary Ammonium Ionic Liquids with Perfluoroalkyltrifluoroborates: Synthesis, Characterization, and Properties. *Chem. - Eur. J.* **2006**, *12*, 2196−2212.

(32) Štejfa, V.; Rohlíček, J.; Červinka, C. Phase behaviour and heat capacities of selected 1-ethyl-3-methylimidazolium-based ionic liquids II. *J. Chem. Thermodyn.* **2021**, *160*, No. 106392.

(33) Štejfa, V.; Rohlíček, J.; Červinka, C. Phase behaviour and heat capacities of selected 1-ethyl-3-methylimidazolium-based ionic liquids. *J. Chem. Thermodyn.* **2020**, *142*, No. 106020.

(34) Wang, R.; Qi, X.; Liu, S.; He, Y.; Deng, Y. A comparison study on the properties of 1,3-dialkylimidazolium tetrafluoroborate salts prepared by halogen-free and traditional method. *J. Mol. Liq.* **2016**, *221*, 339−345.

(35) Mutch, M. L. Thermal Analysis of 1-Ethyl-3-Methylimidazolium Tetrafluoroborate Molten Salt. *ECS Proc. Vol.* **1998**, *1998-11*, 254−260.

(36) Glasser, L. Lattice and phase transition thermodynamics of ionic liquids. *Thermochim. Acta* **2004**, *421*, 87−93.

(37) Tao, D.-J.; Hu, W.-J.; Chen, F.-F.; Chen, X.-S.; Zhang, X.-L.; Zhou, Y. Low-Viscosity Tetramethylguanidinum-Based Ionic Liquids

with Different Phenolate Anions: Synthesis, Characterization, and Physical Properties. *J. Chem. Eng. Data* **2014**, *59*, 4031−4038.

(38) Fei, Y.; Chen, Z.; Zhang, J.; Yu, M.; Kong, J.; Wu, Z.; Cao, J.; Zhang, J. Thiazolium-based ionic liquids: Synthesis, characterization and physicochemical properties. *J. Mol. Liq.* **2021**, *342*, No. 117553.

(39) Bonhôte, P.; Dias, A.-P.; Papageorgiou, N.; Kalyanasundaram, K.; Grätzel, M. Hydrophobic, Highly Conductive Ambient-Temperature Molten Salts. *Inorg. Chem.* **1996**, *35*, 1168−1178.

(40) Kolbeck, C.; Lehmann, J.; Lovelock, K. R. J.; Cremer, T.; Paape, N.; Wasserscheid, P.; Fröba, A. P.; Maier, F.; Steinrück, H.-P. Density and Surface Tension of Ionic Liquids. *J. Phys. Chem. B* **2010**, *114*, 17025−17036.

(41) Tariq, M.; Freire, M. G.; Saramago, B.; Coutinho, J. A. P.; Lopes, J. N. C.; Rebelo, L. P. N. Surface tension of ionic liquids and ionic liquid solutions. *Chem. Soc. Rev.* **2012**, *41*, 829−868.

(42) Anouti, M.; Caillon-Caravanier, M.; Dridi, Y.; Galiano, H.; Lemordant, D. Synthesis and Characterization of New Pyrrolidinium Based Protic Ionic Liquids. Good and Superionic. *J. Phys. Chem. B* **2008**, *112*, 13335−13343.

(43) MacFarlane, D. R.; Forsyth, M.; Izgorodina, E. I.; Abbott, A. P.; Annat, G.; Fraser, K. On the concept of ionicity in ionic liquids. *Phys. Chem. Chem. Phys.* **2009**, *11*, 4962−4967, DOI: 10.1039/b900201d.